RSC Advances

PAPER

View Article Online
View Journal | View Issue

Cite this: *RSC Adv.*, 2026, **16**, 12119

Synergetic effects of inorganic sepiolite filler and electroactive polyaniline on the physical and charge transport properties of polyaniline-layered phosphonated PVA–sepiolite membranes

Fazila Ashraf, Asif Ali Qaiser, * Nida Abid and Samrina Sharif

Thermomechanically stable and cation exchange membranes are desired in high-temperature polymer electrolyte fuel cell (PEMFC) applications. The currently used membranes, such as Nafion®, face stability problems and dehydrate at high temperatures in fuel cells thus losing their efficiency. To develop a thermally stable and highly cation-exchanging membrane, this study elucidates the influence of two structural modifications: the addition of inorganic filler (*i.e.*, sepiolite (SEP)) incorporated in phosphonated polyvinyl alcohol (PVA) membranes and surface layering of electroactive polyaniline (PANI) at the surface. This research specifically elucidates how these modifications affect membranes' physical and charge transport properties. The SEP content was varied from 0.5 to 10%, whereas a thin PANI layer was deposited using *in situ* vapor-phase polymerization of aniline at the surface of crosslinked PPVA matrix membranes. These membranes were characterized using FTIR spectroscopy and dynamic mechanical analysis (DMA) and, ion exchange capacity (IEC), water uptake, and proton conductivity were also measured. The charge transport mechanism was evaluated using electrochemical impedance spectroscopy (EIS). The hydrophilic nature of PANI and SEP enhanced proton conductivity up to 96 mS cm^{-1} at a water uptake of 81%, whereas IEC was measured up to 2.08 meq. g^{-1} at 5% of sepiolite content. The storage modulus and loss tangent showed membrane stability up to 80 °C, with the storage modulus as high as 320 MPa. In the EIS, equivalent circuit modelling was used to study various resistive and capacitive processes at the electrode/membrane interface and through the membrane bulk. SEP content increased bulk membrane capacitive charging owing to higher water retention in the membranes. Surface PANI layering significantly improved the charge transport, reduced the overall resistance, and increased the capacitance by 2–3 orders of magnitude across both electrode and bulk phases. This work validates a strategy for developing robust PEM system for PEMFCs by precisely adjusting physical and charge transport properties.

Received 30th November 2025
Accepted 2nd February 2026

DOI: 10.1039/d5ra09259k

rsc.li/rsc-advances

Introduction

The demand for fuel cell technology is increasing because of its efficiency and lower noise compared to thermal generators, being a non-combustion source in nature (*i.e.*, low carbon footprint).[1–6] Fuel cells usually use hydrogen and yield water as a by-product; therefore, they are considered an attractive and clean technology[7,8] that favours low emission of heat and carbon dioxide.[9] A fuel cell consists of a proton exchange membrane (PEM), gas diffusion, backing, and catalyst layers on the PEM, and an anode and a cathode.[10] The fuel cells are classified based on the type of electrolyte and the fuel, *i.e.*, proton exchange membrane fuel cells (PEMFCs), direct methanol fuel cells (DMFCs), solid oxide fuel cells (SOFCs), *etc.*[11–16] Because of their low operating temperature, rapid startup capabilities, light mass, and excellent power density, PEMFCs are by far the most encouraging fuel cell technology.[17,18] PEMFCs were originally devised to be used in compact distributed power generators, and are now commonly used in portable cellular phones, computers, and transportation.[13,19]

A proton exchange membrane (PEM) is an ionic polymer electrolyte that contains fixed negative charges, allowing it to exchange cations (*i.e.*, protons). It acts as a charge carrier for protons, a separator for reactant gases, and an insulator preventing electrons from flowing across the membrane.[10] Nafion® is the most widely used PEM in PEMFCs, has an aliphatic perfluorinated backbone and covalently bonded sulfonated cation exchange sites showing long-term stability in both oxidative and reducing environments,[20] however, it loses performance at temperatures above 100 °C.[21,22] Because of the dehydration and the consequent reduction in the number of water-filled

Department of Polymer and Process Engineering, University of Engineering and Technology, Lahore, Pakistan. E-mail: asifaliqaiser@uet.edu.pk

channels, Nafion® membranes exhibited low proton conductivity at high temperature (>100 °C).[23,24]

Researchers have proposed adding plasticisers, fillers, and polymeric materials to overcome this dehydration issue. Nafion® membranes incorporated with inorganic fillers, such as phosphotungstic acid, exhibited strong proton-transfer reactions and improved capacity to retain water by lowering the vapor pressure when the level of free water is low in the cell. Therefore, Nafion® composite membranes by incorporating additives proved to be effective in 110–120 °C temperature range.[10,24,25] Various polymeric materials have been tested primarily to reduce production cost while preserving the mechanical and conductivity properties similar to those of Nafion® for low temperature (60–80 °C) conditions.[1] Hydrocarbon-based polymer blend membranes have been widely explored as low-cost alternatives to perfluorinated ionomers. For example, Elnaggar *et al.* reported sulfonated polyvinyl chloride (SPVC)/polymethyl methacrylate (PMMA)/polystyrene sulfonate (PSS) blend membranes demonstrating enhanced proton conductivity (up to 4.7×10^{-2} S cm^{-1}), increased ion exchange capacity, and significantly reduced methanol permeability compared to Nafion® 117. Their study highlighted the effectiveness of polymer sulfonation and blending strategies in improving proton transport and fuel barrier properties. However, such bulk-modified systems primarily rely on ionic group density and water uptake, which may limit dimensional stability at elevated operating temperatures. These observations motivated the development of alternative membrane architectures that combined efficient proton conduction with improved thermal and dimensional stability.[26] Tamer *et al.*,[27] developed sulfonated chitosan/alginate composite membranes and successfully achieved water uptake and methanol permeability of 31.86% and 1.9×10^{-9} g cm^{-2} s^{-1}, respectively. These properties are comparable to Nafion®-117 membranes that usually showed water uptake and methanol permeability of 21.30% and 2.76×10^{-8} g cm^{-2} s^{-1}, respectively.[19,24]

Polyvinyl alcohol (PVA) is a promising, cost-effective, and biocompatible substitute to high-value materials like Nafion; however, pristine PVA is hygroscopic and lacks the necessary ion conduction properties. These properties can be engineered through functionalization processes such as sulfonation or phosphonation. A notable example is sulfonated poly(glycidyl methacrylate-*co*-styrene) [SP(GMA-*co*-ST)],[28] which was successfully synthesized *via* free radical polymerization and functionalized using sodium sulfite. Although such sulfonated copolymers are effective for ionic interaction, demonstrated by their ability to facilitate 'proton change' through negatively charged sulfonic acid groups (–SO_3H), they often rely on high hydration levels for conductivity. In contrast, phosphonation offers a distinct advantage for PEMFC applications, as it can maintain ionic conductivity even at lower hydration levels with superior thermal stability.[29]

Polyaniline (PANI) deposition on base membranes as a layer enhances proton conductivity because of its unique electrochemical characteristics.[24] The physicochemical nature and chemical stability of PANI allow ions passage through the composite membranes using PANI's polarization clusters. These clusters can generate a pathway for cations similar to that of Nafion® membranes.[25] Qaiser *et al.* studied the effect of PANI deposition extent on ionic conductivity of mixed cellulose ester membranes through polaron/bipolaron transitions of PANI.[24] Sun *et al.* fabricated composite membranes based on PANI–polybenzimidazole (PBI) and obtained a proton conductivity of 0.13 S cm^{-1} at 180 °C in fully hydrated conditions.[30] Escudero-Cid *et al.* modified Nafion®-117 membrane with PANI for DMFC and reduced the methanol crossover from 2.55×10^{-6} to 2.08×10^{-7} cm^2 s^{-1} with improvement in proton conductivity.[31]

Inorganic sepiolite (SEP) filler has unique characteristics because of the presence of octahedral magnesium sheet and silane groups in the structure (Fig. 1) that can retain water at high temperature and maintain good mechanical properties of the composite membranes. SEP has been added to various membranes, such as sulfonated polyether ether ketone (SPEEK)[32] and sulfonated polyether sulfone octyl sulfonamide (SPEOS)[33] for improved mechanical and ion exchange properties.[32]

In this work, we report a novel composite membrane system based on polyvinyl alcohol (PVA) functionalized with phosphonate groups and reinforced with SEP clay as an inorganic filler. The previous studies mainly focused on either SEP-filled PPVA membranes[34,35] or polyaniline (PANI)-modified[25,31] proton exchange membranes (PEMs) independently, this study uniquely combines both strategies by applying a uniform PANI coating *via in situ* vapor-phase polymerization. The phosphonate functionalization of PVA matrix enhances proton conduction and crosslinking density, which, together with the incorporation of SEP, significantly improves the membrane's thermal and dimensional stability[36,37] under hydrated, high-temperature fuel cell operating conditions. The superior water retention and mechanical benefits of sepiolite fillers in membranes have been reported earlier but the synergistic effects of simultaneous inorganic filler (SEP) incorporation and electroactive polymer (PANI) surface modification remained largely unexplored. Here, we systematically investigated how this dual modification through phosphonate-functionalized SEP/PVA composite formation, combined with surface PANI layering, affects the physicochemical, structural, and electrochemical properties of the membranes. These findings provide new insights into the design of robust, high-performance PVA-based PEMs for proton exchange membrane fuel cells (PEMFCs) applications.

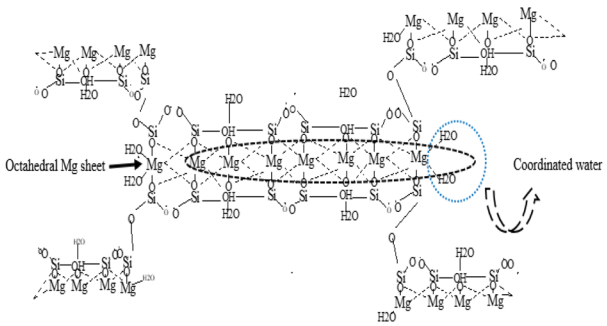

Fig. 1 Schematic representation of sepiolite structure.

Experimental

Material

Phosphonated polyvinyl alcohol (PPVA) membranes containing 0.5%, 2%, 5% and 10% of sepiolite (SEP) were kindly provided by Prof. A. R. Irfan's group at Gazi University, Türkiye. These membranes were prepared as mentioned elsewhere.[38] To modify SEP–PPVA membranes with polyaniline and subsequent characterizations, aniline, ammonium persulfate (APS), sodium hydroxide (NaOH), and phenolphthalein were acquired from Merck USA. Distilled water was used in all preparations.

Vapor phase deposition of polyaniline (PANI) on PPVA–sepiolite membranes

For vapor-phase deposition of PANI on the surface of SEP–PPVA, the base membranes were soaked in 0.8 M anilinium solution (*i.e.*, aniline in 0.4 M HCl) for 10 min, surface-wiped with blotting paper, and then hung in a closed bottle containing APS solution (0.3 M of ammonium persulfate in 3 M HCl). The APS solution was heated to 55–60 °C, and the membranes were kept inside the bottle for 10–15 min for *in situ* polymerization of aniline present on the surface of the base membranes, reacting with APS vapours (Fig. 2). This reaction yielded a uniform coating of dark green colour covering the surface confirming PANI coating on PPVA–sepiolite membranes in its emeraldine salt state.[24]

The membranes are identified as *x*SEP–PPVA/PANI, where *x* denotes the percentage of sepiolite in the membranes.

Membrane characterization

Scanning electron microscopy (SEM)

For morphological analysis of SEP–PPVA and SEP–PPVA/PANI composite membranes, ZEISS SIGMA 500VP scanning electron microscope was used at 5000× magnification at 2 kV.

Fourier transform infrared spectroscopy (FTIR)

JASCO FTIR 4100 in ATR mode was used for surface chemical characterization of the membranes in the wave number range 400–4000 cm^{-1} and at a scan rate of 4 cm^{-1} s^{-1}.

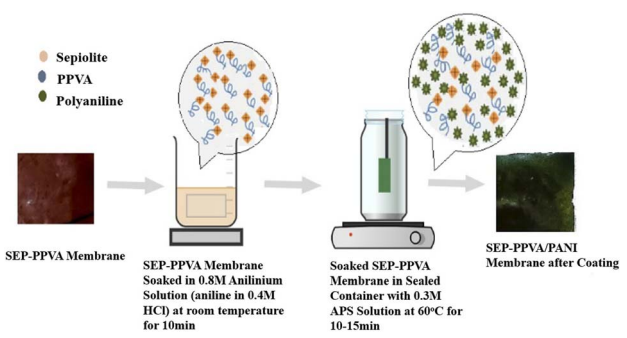

Fig. 2 *In situ* vapor-phase deposition of PANI on SEP–PPVA membranes.

Dynamic mechanical analysis (DMA)

TA Q800 DMA was used to assess the thermomechanical stability of the membranes in tensile mode using temperature step of 2 °C min^{-1}. Membrane samples were cut according to ASTM D4065 in a rectangular shape of 50 × 6 mm size, and a frequency of 1 Hz was imposed to measure storage modulus and loss tangent, *i.e.*, E' and $\tan\delta$, respectively, at various temperatures.

Water uptake

Water uptake of SEP–PPVA and SEP–PPVA/PANI membranes was measured by immersing membranes in deionized water, equilibrated to a constant wet weight (W_{wet}). The membranes were dried in an oven at 60 °C for 4 h[39] and weighed again (W_{dry}).[40,41] Water uptake was calculated by using the following eqn (1):

$$\%\ \text{water uptake} = \frac{W_{wet} - W_{dry}}{W_{dry}} \times 100 \quad (1)$$

Ion exchange capacity (IEC)

Ion exchange capacity (IEC) of SEP–PPVA and SEP–PPVA/PANI membranes was evaluated using indirect titration method.[40,41] Membranes were cut into 1 cm^2 strips and immersed in 1 M HCl for 24 h at room temperature to attract H^+ ions on the surface. Excess H^+ ions were removed by soaking in deionized water, and the membranes were placed in desiccators until dried to a constant weight (W_{dry}). These dried membranes were submerged in a 2 M NaCl solution for 24 hours to exchange H^+ with Na^+ ions. Phenolphthalein was used as an indicator to titrate the mixture containing Na^+ ions with 0.01 M NaOH. The IEC was computed using eqn (2).[39]

$$\text{IEC} = C_{NaOH} \times \frac{V_{NaOH}}{W_{dry}} \quad (2)$$

where, C_{NaOH} = concentration of NaOH, V_{NaOH} = volume of NaOH solution used, W_{dry} = weight of dry membranes.

Proton conductivity and electrochemical impedance spectroscopy (EIS) study

Proton conductivity was computed using Gamry® (Interface 1000) Potentiostat by interposing water-soaked membranes between two gold-plated discs in a two-electrode set-up (Fig. 3). A 100 mV AC was applied in the frequency range 1 MHz to 0.01 Hz as an input signal. The ionic conductivity was calculated by noting the resistance from the Nyquist plot and using the following equation:[42,43]

$$\text{Proton conductivity} = \frac{L}{RA} \quad (3)$$

where, L = wet membrane thickness, R = membrane resistance, A = surface area of electrodes.

To study the charge transport and charge transfer characteristics of SEP-PPVA and SEP-PPVA/PANI composite membranes using EIS, equivalent circuit modelling was applied

L= Wet membrane thickness,
R= Membrane resistance,
A= Surface area of electrodes.

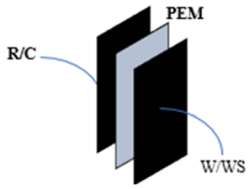

Fig. 3 Schematic of EIS setup for the measurement of proton conductivity.

to the data. Nyquist plots were used for modelling and interpreting various electrochemical processes within the membranes.

Results and discussion

Scanning electron microscopy (SEM)

Fig. 4a and b show SEM surface micrographs of unmodified sepiolite-filled phosphonated PVA (SEP–PPVA) membranes containing 0.5 and 10 wt% sepiolite, respectively. At low filler loading (0.5 wt%), the membrane surface appeared relatively smooth and homogeneous, indicating effective dispersion of sepiolite within the phosphonated PVA matrix and good polymer filler compatibility (Fig. 4a). Such uniform morphology is desirable for proton exchange membranes, as it minimizes localized defects and promotes continuous ion-transport pathways. In contrast, increasing the SEP content to 10 wt% (Fig. 4b) resulted in a rougher surface with visible agglomerates and surface-enriched filler domains, suggesting partial filler migration and increased filler–filler interactions at higher loadings. Although, this surface heterogeneity might compromise morphological uniformity, the exposure of hydrophilic SEP domains was expected to enhance water retention and dimensional stability under hydrated PEMFC operating conditions.

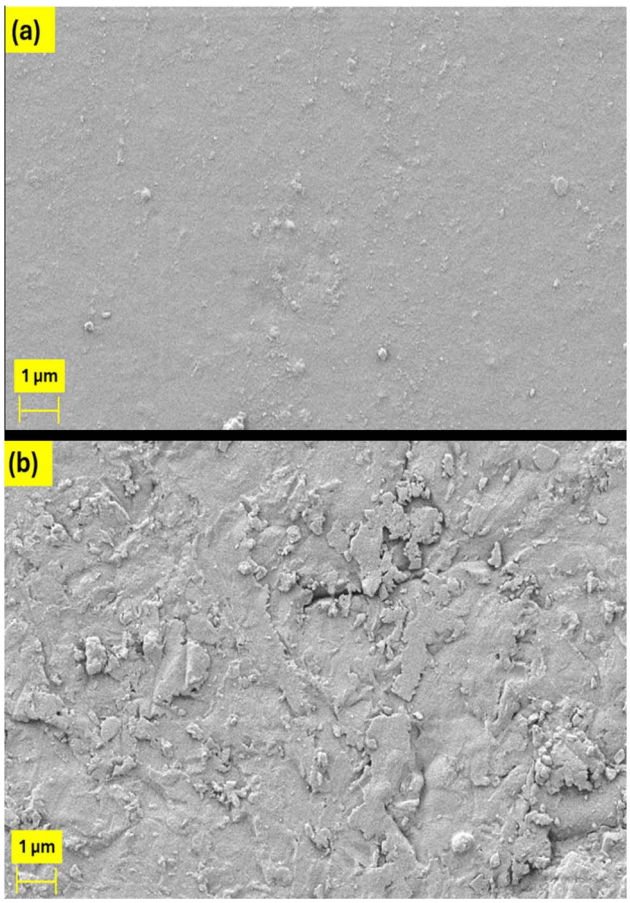

Fig. 4 SEM Micrographs of SEP-PPVA composite membranes (a) 0.5% SEP-PPVA (b) 10% SEP-PPVA.

SEM images of PANI-modified membranes (Fig. 5a and b) revealed a clear morphological evolution following *in situ* vapor-phase polymerization of aniline on SEP–PPVA substrates. For membranes containing 2 wt% SEP, PANI deposition resulted in a comparatively uniform and continuous surface layer compared to the uncoated membrane, indicating that vapor-phase polymerization enabled conformal surface modification without disrupting the underlying composite structure. The coating morphology is characterized by interconnected granular features of polyaniline in its emeraldine salt form,[44] suggesting effective surface-confined polymer growth initiated by aniline absorbed within the membrane surface. At higher magnification (Fig. 5b), localized microcracks were shown within PANI layer, which might arise from the intrinsic rigidity of doped PANI combined with drying-induced stresses and elastic mismatch between the coating and the flexible SEP–PPVA substrate. The PANI layer remained largely continuous and adhered to the surface of the base membrane. Partial removal of the coating (Fig. 5a) suggested a PANI layer approximately 400–500 nm, consistent with a thin electroactive surface layer rather than bulk incorporation. The SEM morphology confirmed the formation of a hierarchically structured membrane architecture in which the bulk SEP–PPVA matrix governed water management and dimensional stability, whereas the surface PANI layer modified interfacial charge-transport characteristics. These distinct morphological features suggest that SEP primarily governs bulk structural integrity, whereas the PANI layer contributes mainly to surface continuity, indicating distinct but potentially cooperative roles for PEMFC applications.

Fourier transform infrared spectroscopy (FTIR)

FTIR spectra of SEP–PPVA and SEP–PPVA/PANI membranes showed phosphonation of PVA, presence of aminopropyl triethoxy silane (APTES) modified SEP, and PANI layering on the membranes. In FTIR spectra of SEP–PPVA composite membranes, the major peaks for phosphonation of PVA appeared at 915 cm^{-1} and 1005 cm^{-1}, indicating vibrational stretching of P–OH bond (Fig. 6a)[45] whereas the characteristic peaks of SEP at 950–1250 cm^{-1} indicated vibration of Si–O–Si linkage. Characteristic vibrations of the octahedral–tetrahedral

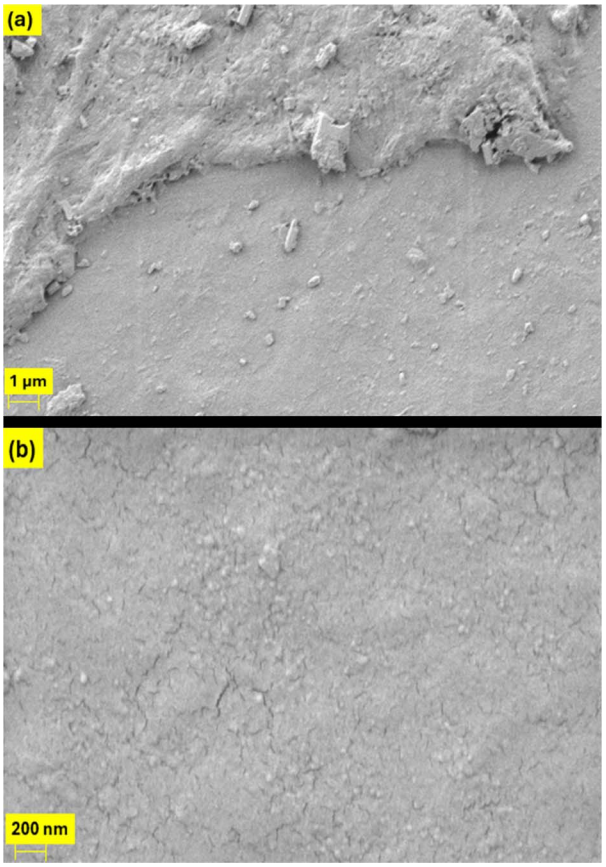

Fig. 5 SEM micrographs of SEP–PPVA/PANI membranes with 2% SEP content at different scales (a) 1 μm (b) 200 nm.

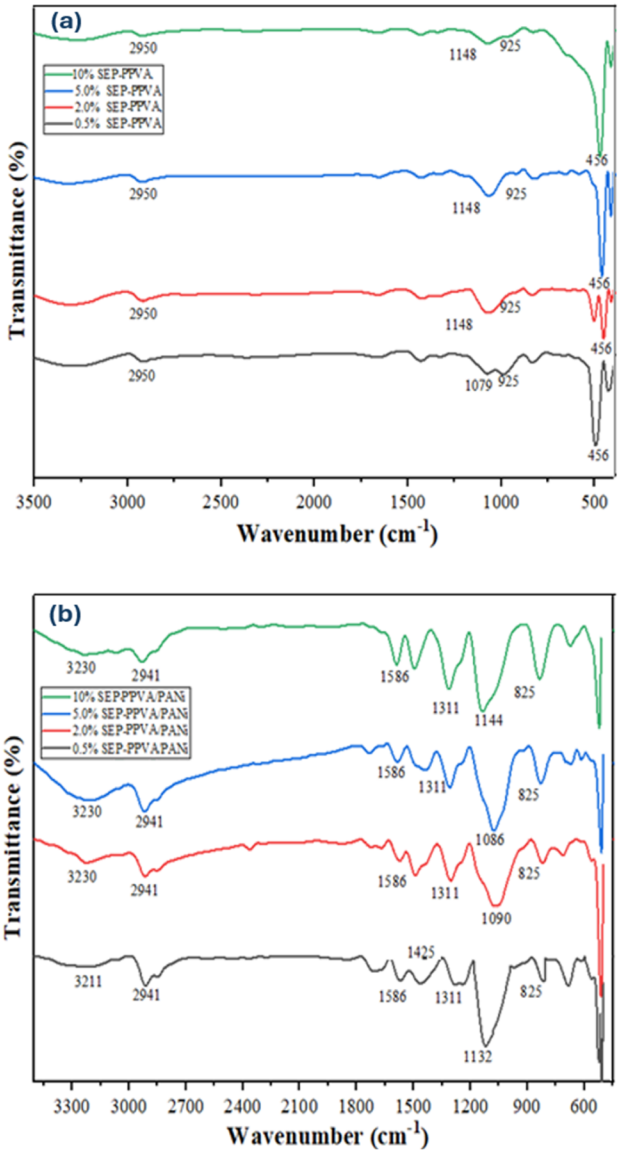

Fig. 6 FTIR spectra of composite membranes (a) SEP–PPVA (b) SEP–PPVA/PANI.

linkage of Si–O–Mg and Mg–Mg–OH in SEP were shown at 450 cm^{-1} and 650 cm^{-1}, respectively, whereas the bending peak at 1663 cm^{-1} indicated the presence of OH group of zeolitic water. Organic molecules interacting with fibrous silicates are often identified at 1200–2000 cm^{-1}. Typical amine bands at 1600 cm^{-1} confirmed the grafting of aminopropyl triethoxy silane (APTES) on fibrous SEP particles.[46,47] The absorption band at 2950 cm^{-1} was associated with C–H stretching vibration of coupling agent aminopropyl triethoxy silane groups. All these observations support the grafting of APTES onto the SEP surface.[48,49] The strong IR bending vibration at 495 cm^{-1} indicated the presence of O–Si–O in SEP and its interaction with $-PO_4^{3-}$ in PPVA matrix.[32]

The polaronic structure *i.e.*, π-electron delocalization of PANI was shown at 1306 cm^{-1} whereas the IR absorption peaks at 1235 cm^{-1} and 1152 cm^{-1} represented –C–N^+ and –NH^+= stretching, respectively. The quinonoid and benzenoid stretching were observed at 1568 and 1425 cm^{-1}, respectively, which are the prominent peaks to identify emeraldine oxidation state of PANI layer at the surface of the membranes.[50] The quinonoid peak indicated emeraldine salt (ES) state of PANI, and the polaron band conjugation at 1133 cm^{-1} showed the ability of PANI to create a passage for the conduction of ions through the membrane.[50] The IR peak of $-CH_2$ groups in PPVA appeared at 2912 cm^{-1}, and a peak shift from 1148 to 1090 cm^{-1} showed ionic interaction of the $-NH_2$ group of PANI with the phosphonic group of PPVA.[51]

PANI deposition on the surface and its hydrogen bonding[52] with phosphoric acid groups of PPVA can be clearly seen in the range of 1132–1586 cm^{-1} (Fig. 6b) and these interactions promote ionic conduction through the membranes as proposed in Fig. 7. Hydrogen bonding between H atoms of PANI and OH of PPVA provides the adherence stability of PANI layer at the surface of the base membranes,[53] and strong bonding of $-PO_4^{3-}$ and PANI also plays a role in the stable layering of PANI at the surface.

Dynamic mechanical analysis (DMA)

Dynamic mechanical analysis is used to study the mechanical stability of the composite membranes with respect to thermal

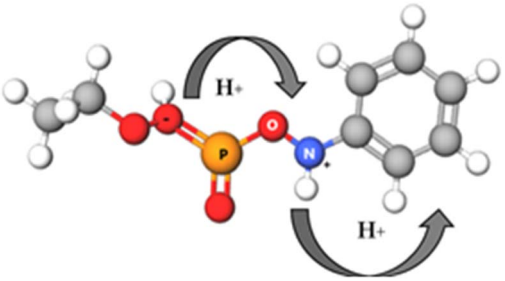

Fig. 7 Proposed possible interaction of PPVA and PANI.

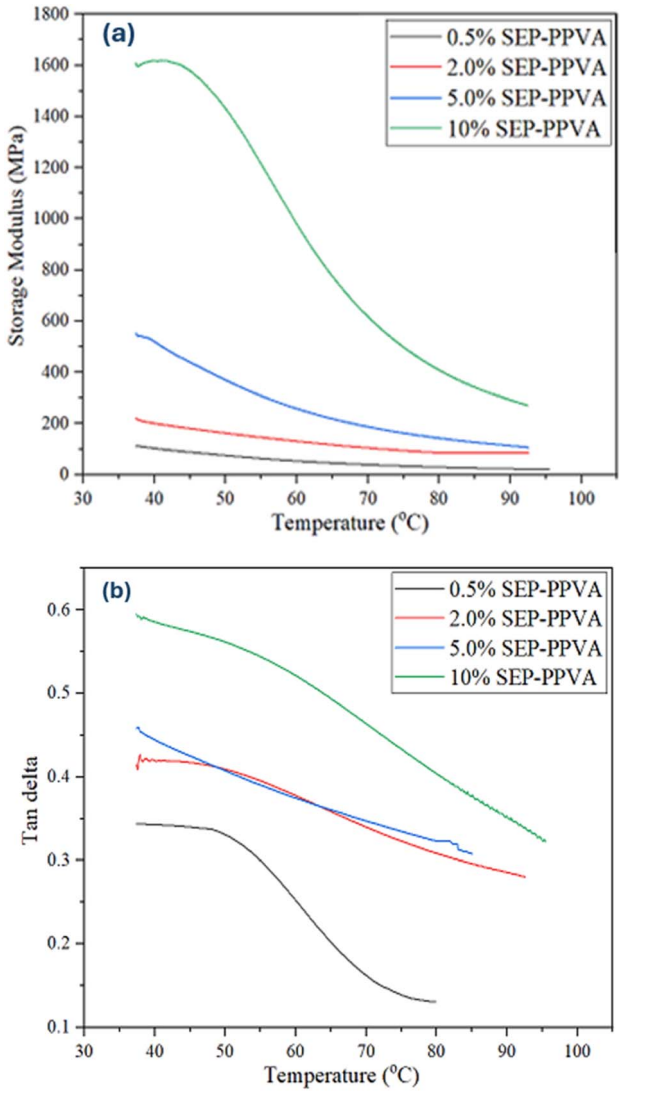

Fig. 8 DMA graphs of SEP–PPVA composite membranes: (a) storage modulus *vs.* temperature, (b) tan δ *vs.* temperature.

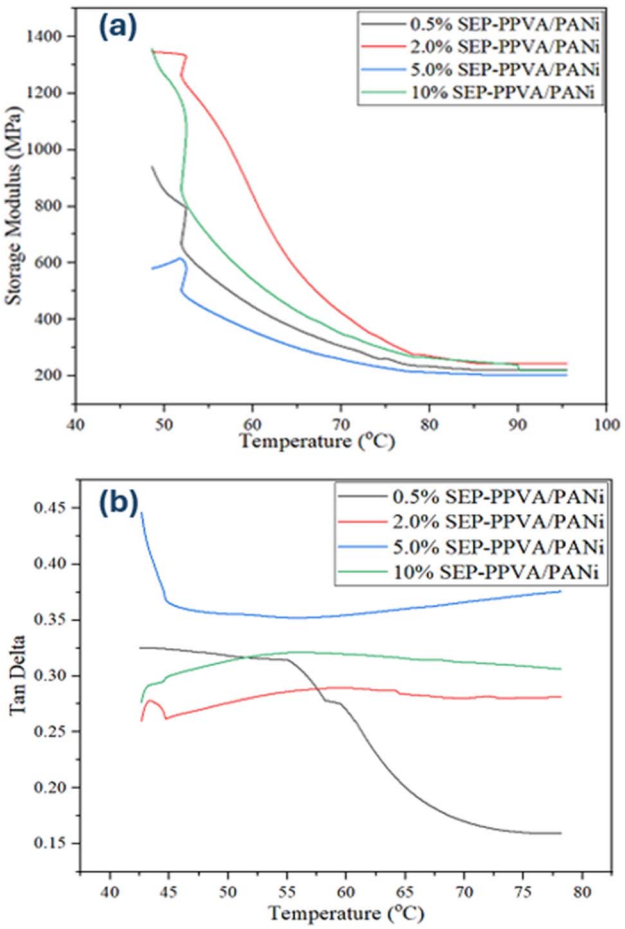

Fig. 9 DMA of SEP–PPVA/PANI composite membranes: (a) storage modulus *vs.* temperature, (b) tan δ *vs.* temperature.

history. Fig. 8 and 9 show storage modulus and loss tangent (tan δ) to assess mechanical stability and glass transition of the composite membranes. In Fig. 8a and b, effect of SEP content in PPVA matrix is shown in terms of storage modulus and tan δ, where storage modulus increased significantly and tan δ also increased in the temperature range 50 to 63 °C as SEP content increased from 0.5 to 10%. This increase may be attributed to the physical crosslinking of PPVA with SEP, which imparted mechanical stability at temperatures above 60 °C. Above this temperature, the storage modulus decreased abruptly due to an intrinsic thermal softening of PPVA matrix. This indicates the temperature-dependent mechanical stability of polymer framework, resulting in diminished mechanical strength as the thermal energy increases. In the case of 2% and 5% SEP content, an overlapping behaviour in tan δ was observed that showed an insignificant effect of filler loading in this range. The change in tan δ with temperature shows the state of molecular chain mobility, and thus a peak in tan δ shows the glass transition temperature (T_g).[53,54]

Fig. 8b shows T_g around 50 °C for 0.5% sepiolite content in PPVA membrane that shifted to 63 °C for 10% sepiolite content. This demonstrates a pronounced effect of SEP content on the viscoelastic properties of the composite membranes. The strong influence is also evident in the storage modulus, which indicates the effect of increasing SEP content (0.5–10%). The reinforcing effect of SEP made it stable only up to 50–60 °C, and then dropped rapidly. The storage modulus appeared constant at 350–200 MPa for 0.5–5% SEP content at 65–80 °C, and 10%

SEP showed gradual decrease after 65 °C (Fig. 8a). The decrease in storage modulus might occur due to the agglomeration of SEP in PPVA.[32] Increase in storage modulus at lower temperature might be due to strong interfacial interaction between SEP particles and PPVA molecular chains (*i.e.*, hydrogen bonding between $-PO_4^{3-}$ and SEP).[32] The drop in storage modulus with temperature also depends on SEP content because, as a clay, it settles between the molecular chains and weakens interchain molecular bonding.[32,55]

In literature, the storage modulus of pristine PVA was reported around 136 MPa (ref. 55) and hygroscopicity and mechanical stability of SEP suppressed the viscous effect of PVA showing temperature stability up to 63 °C.

Surface deposition of PANI also influenced the mechanical properties of composite membranes. The tan δ dropped from 0.6 (SEP–PPVA) to 0.372 (SEP–PPVA/PANI) probably due to oxidative conditions during *in situ* PANI layering that might result in molecular chain cleavage of PPVA. Because of the brittle nature of PANI, the storage modulus increased, but a significant shift was observed in tan δ as shown in Fig. 9a and b. At 10% SEP–PPVA, the storage modulus was 1600 MPa indicating mechanical stability because of SEP, whereas it decreased to 1400 MPa in the case of PANI layering, probably due to free radical cleavage of PPVA chains in the presence of strong acidic conditions of aniline polymerization. The storage modulus increased from 0.5% to 5% SEP content due to the synergistic effect of SEP filler and the high modulus of brittle of the PANI layer, as indicated in SEM images as well. These results showed that the 10% SEP may be the optimum content for the best mechanical properties in terms of storage modulus and tan δ.[15] The irregularity in the results of SEP–PPVA/PANI membranes may be attributed to uneven PANI coating (Fig. 9) and a typical hetero-phase behaviour of composite membranes. In summary, the brittle PANI layer might bring surface instability and probably cracked under thermal and mechanical stresses. The decay in mechanical properties[25] can be attributed to the hetero-phase effect of SEP–PPVA and PANI layer.[25]

Water uptake

Water uptake plays a crucial role in PEM for promoting proton conductivity, as hydronium ions (H_3O^+) and hydrogen pass through the membrane by connecting with water molecules and diffuse to the cathode side in the fuel cell.[56] Excessive dehydration of the membrane in a fuel cell leads to brittleness and excessive hydration can cause swelling, ultimately affect the membrane electrode assembly (MEA) and leading to flooding within the fuel cell.[19] Pristine PVA demonstrated 210% water uptake whereas PPVA with 30% phosphonation showed a significant reduction to 75%.[29] Incorporation of SEP to PPVA membranes enhanced hygroscopicity, as these membranes can retain water at elevated temperatures.[57] The hydrophilic fibrous structure of SEP provides abundant water anchoring sites, as evident in the increased water uptake observed for SEP–PPVA membranes. For example, 2 wt% SEP–PPVA membrane exhibited 87.5% water uptake notably higher than that of pristine PPVA.[29] The water uptake increased with incorporation of SEP up to 5 wt% and then declined slightly at 10 wt% to 79.5%. This decrease can be attributed to the immobilization of $-PO_4^{3-}$ sites that might have occurred due to crosslinking of PPVA with SEP[29,58] as well as due to the agglomeration of SEP particles that reduced the availability of hydrophilic sites.[59] Surface modification with PANI further increased water uptake of SEP–PPVA membranes. This 90% water uptake in SEP/PPVA–PANI membranes is associated with the hydrophilic nature of PANI's emeraldine salt state and open fibrillar like structure.[60] The water molecules association originates from the strong hydrogen bonding between quinoid sites ($-N^+=$) of PANI and phosphonate ($-PO_4^{3-}$) groups in PPVA that resulted in hydrophilic membranes with improved proton conductivity and water uptake.[60] Essentially, this fibrillar nature of PANI can provide the stable network that can compensate the physical rigidity of membranes by maintaining the hydration at 10 wt% of SEP loading.[61] Table 1 summarizes the water uptake, ion exchange capacity (IEC), and proton conductivity values for the various membranes studied. Notably, SEP–PPVA/PANI membranes demonstrated consistently higher water uptake compared to SEP–PPVA composite membranes at corresponding SEP loadings, underscoring the cooperative role of PANI and SEP in promoting membrane hydration.

These results indicate that SEP contributes primarily to bulk water retention and mechanical stabilization, the PANI layer plays a crucial role in surface hydration and ionic conduction pathways, consistent with the proposed proton conduction mechanism illustrated in (Fig. 10). This complementary interaction likely leads to enhancements in overall membrane hydration and conductivity beyond the additive effects of individual components.

Ion exchange capacity (IEC)

Ion exchange capacity is a key indicator of ionizable protons (H^+) or active sites available in the membrane matrix, directly influencing the proton transport efficiency in PEMs. Table 1 summarizes the IEC values of SEP–PPVA and SEP–PPVA/PANI composite membranes as a function of SEP loading. It has been previously reported that the inclusion of PVA in Nafion membrane can reduce the IEC value of pristine Nafion from 0.93 meq. g^{-1} to 0.58 meq. g^{-1} due to crosslinking that masks the ionizable sulfonic groups through covalent binding, thereby decreases the available proton sites.[62,63] Pristine PPVA membranes exhibited an IEC value up to 2.1 meq. g^{-1}, attributed to the abundance of phosphonate groups.[29] In the case of SEP loading, IEC values showed a nonlinear relationship between SEP loading and PPVA. IEC values decreased to 0.91 meq. g^{-1}, indicating the reduction of free-ion exchange sites through the crosslinking.[59] Increasing the SEP content to 5 wt%, led to increase in IEC value to 1.27 meq. g^{-1}. This specific enhancement might stem from the optimized dispersion of the filler in matrix that created additional ion exchange sites or percolation pathways for increased ionic mobility. However, the IEC value decreased to 0.96 meq. g^{-1} at 10 wt% of SEP, probably due to agglomeration and excessive cross-linking sites. Despite

Table 1 Water uptake, IEC and proton conductivity of SEP–PPVA and SEP–PPVA/PANI composite membranes

Composite membranes	Water uptake (%)	IEC (meq. g^{-1})	Proton conductivity (mS cm^{-1}) (water-soaked)	Proton conductivity (mS cm^{-1}) dry membrane
0.5% SEP–PPVA	67.5	0.91	25.0	5.8
2% SEP–PPVA	87.5	1.12	30.0	4.9
5% SEP–PPVA	81.8	1.27	75.0	6.1
10% SEP–PPVA	79.5	0.96	17.0	3.2
0.5% SEP–PPVA/PANI	64.5	0.92	50.4	7.0
2% SEP–PPVA/PANI	73.6	1.18	62.3	7.4
5% SEP–PPVA/PANI	80.7	2.08	96.3	6.5
10% SEP–PPVA/PANI	89.6	1.20	45.2	1.6
SPEEK/SEP[32]	12.3	1.51	199	—
SPEEK/PANI[60]	45.1	1.44	—	—

this decrease, IEC values are in the range required for PEMFCs.[39,49]

Surface modification with PANI membranes yielded a substantial increase in IEC values. Specifically, at 0.5 wt% SEP loading, the IEC increased from 0.91 meq. g^{-1} to a maximum of 2.08 meq. g^{-1} at 5 wt% SEP. This increase was largely driven by the intrinsic hydrophilic nature of the emeraldine state of PANI, and due to the robust hydrogen bonding and electrostatic interactions of quinoid nitrogen sites of PANI and phosphonate groups of PPVA.[57] Collectively, these interactions facilitated in providing the additional protonatable sites and increased ion transport. At higher SEP loading (10 wt%), a reduction in IEC to 1.20 meq. g^{-1} was observed for SEP–PPVA/PANI membranes. This decline was likely a consequence of filler agglomeration and an increase in crosslink density. These factors can reduce the accessibility of ion exchange sites. This trend emphasizes maintaining a critical balance between filler content and membrane microstructure that can provide the optimal threshold that may favour the continuous pathways necessary for efficient ion transport.

Furthermore, SEP acts as a reservoir for structural water, maintains the hydration for proton hopping, whereas PANI contributes to the essential active sites for charge transport. These interactions indicate a significant improvement over unmodified SEP–PPVA membrane systems.

Overall, SEP incorporation governs the structural and crosslinking environment in the membrane matrix, whereas PANI improves IEC values by facilitating a more efficient conduction network allowing the SEP–PPVA/PANI membranes to show superior characteristics as compared to the unmodified SEP–PPVA membrane system.

Proton conductivity

The proton conductivity serves as a vital performance indicator for PEMs as it defines the efficiency of PEMFCs. Proton conductivity values for SEP–PPVA and SEP–PPVA/PANI membranes were measured under both dry and water-soaked conditions, as given in Table 1.

Previous studies have reported proton conductivity of pristine PPVA 20–30 mS cm^{-1} at a phosphonation degree of 30%.[29] The addition of SEP, being inorganic fibrous clay, influenced the proton conductivity in a complex manner. For 5 wt% SEP loading, the highest proton conductivity values *i.e.*, 6.1 mS cm^{-1} and 75 mS cm^{-1} were achieved in dry and soaked conditions, respectively. This increase can be attributed to the unique fibrous structure of SEP clay, which can create water tunnels to support the vehicular transport mechanism of hydronium ions (H_3O^+) and hydrogen (H^+) ions through the membranes.[59] Hygroscopic SEP supported the proton conductivity of 75 mS cm^{-1} at 5% sepiolite content in soaked conditions, indicating absorption of water by sepiolite that created water tunnels for protons and promoted the vehicular mechanism for high proton conductivity.[33]

Phosphonated sites ($-PO_4^{3-}$) have a unique amphoteric character, capable of accepting or donating the protons, thus supporting the proton hopping from a hydrodynamic bond to facilitate proton conduction even at low hydration and/or at elevated temperatures.[45] The proton conductivity in SEP–PPVA membranes in dry condition increased up to 5% SEP loading but dropped beyond this loading due to agglomeration and increased crosslinking density between PPVA and SEP. These factors can restrict ionic pathways and hinder proton mobility.

Surface modification with PANI further enhanced proton conductivity in SEP–PPVA/PANI composite membranes in both dry and hydrated states. The intrinsic polaron and bipolaron

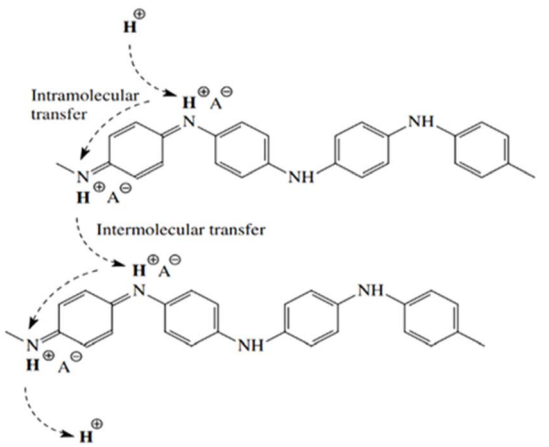

Fig. 10 Proposed proton conduction mechanism in PANI.

network of PANI, alongside the imine sites, allows simultaneous proton and electron transport through an electrochemical redox process. This cooperative process (Fig. 10) enhances charge carrier density and improves ionic flux through the composite structure. Additionally, the fibrillar morphology and hydrophilic nature of emeraldine PANI state create continuous proton-conducting channels, improving water retention and proton hopping efficiency.

The synergistic interaction between SEP and PANI was shown by proton conductivity of 93.3 mS cm^{-1} that was observed at 5 wt% SEP in the hydrated state. This synergistic effect arises from the combined contributions of SEP's water-retention tunnels and channel-forming properties, the dynamic proton exchange facilitated by PPVA's phosphonate groups, and the proton–electron transport capability of PANI amine moieties. However, increasing the SEP content beyond 5 wt% produced SEP particle agglomeration, as also shown by SEM micrographs (Fig. 4b) that disrupted proton-conducting pathways by blocking water channels and reduced effective surface area, leading to decreased conductivity.

Electrochemical impedance spectroscopy (EIS) of composite membranes

The electrochemical properties of SEP–PPVA and SEP–PPVA/PANI membranes were evaluated using EIS to evaluate and quantify charge transport and charge transfer processes in SEP–PPVA and SEP–PPVA/PANI composite membranes. Fitting experimental data to an appropriate equivalent circuit elucidates underlying electrochemical processes within the membrane systems. Impedance spectroscopy results are usually represented in Nyquist plot where real component (Z_r) at x-axis denotes the resistance whereas the imaginary component (Z_i) at y-axis represents capacitive properties of an electrochemical system.

In electrochemical systems, such resistive–capacitive type processes are modelled using equivalent circuits (ECs). In equivalent circuits, different physical processes are described using simple electrical elements such as resistors (R), capacitors (C), inductors (L), and constant-phase elements (Q). A dynamic–kinetic process may be modelled by utilising various equivalent circuit elements for composite membranes, as shown in Fig. 13 and 14. The uncompensated resistance (R_0) represents bulk resistance of the electrolyte and electrode. R_1 corresponds to the charge transfer resistance at the electrode and electrolyte interface associated with the redox reactions of polyaniline (PANI). R_2 is related to ionic diffusion and charge transport within the PANI film. The constant phase elements Q_1 and Q_2 describe non-ideal capacitive behaviour arising from surface roughness, structural heterogeneity, and distributed relaxation processes, where Q_1 reflects interfacial capacitance and Q_2 represents the pseudocapacitive response of the PANI matrix. In case of composite membranes, capacitor is replaced by constant phase elements (Q) to represent surface roughness of the membranes. SEP–PPVA membranes at different SEP content showed a typical electrochemical behaviour with varying impedance levels. The impedance scale of real (Z_r) and imaginary components (Z_i) exhibited an increasing–decreasing trend by changing sepiolite content corresponding to water uptake and IEC values, whereas impedance decreased by PANI layering (Fig. 14). This showed a noteworthy contribution of SEP in charge conduction in these membranes with the combined effects of PANI on the surface. This charge conduction involves both resistive (Z_r) and charge-storing capacitive conduction (Z_i) in composite membranes.

In the Nyquist plots of various PPVA composite membranes, the curve identifies a characteristic frequency (ω^*), that is associated with the charge transfer process and given by $\tau = 1/\omega^*$. Each semicircle is characterized by a relaxation time τ that can be defined as the time required for the charge transport in a parallel R–C (resistor–capacitor) element *i.e.*, RC (Fig. 11).

The impedance of this RC circuit, shown in Fig. 11, is given by,

$$Z = \frac{R}{1+\omega^2C^2R^2} - \frac{j\omega CR^2}{1+\omega^2C^2R^2} \quad (4)$$

where R, C, ω and j represent resistance, capacitance, angular frequency ($\omega = 2\pi f$, f = linear frequency), and $\sqrt{-1}$, respectively.

The combined resistive and capacitive behaviour of membranes is depicted as distorted semicircles in Fig. 13 and 14. At high frequency, the suppressed semicircle may be attributed to distributed resistance offered by membranes due to irregular and inhomogeneous dispersion of filler or incomplete PANI coating, which is modelled by a constant phase element (Q). A cation exchange membrane conducts cations through it, whereas electrons are transferred at the membrane/

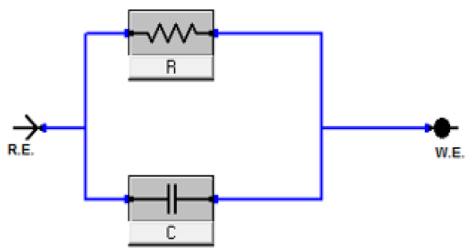

Fig. 11 Parallel circuit model of resistor and capacitor.

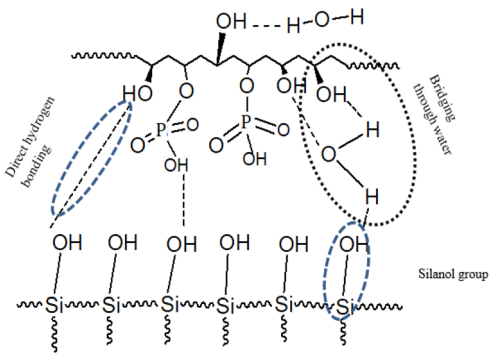

Fig. 12 Proposed interaction of SEP and PPVA.

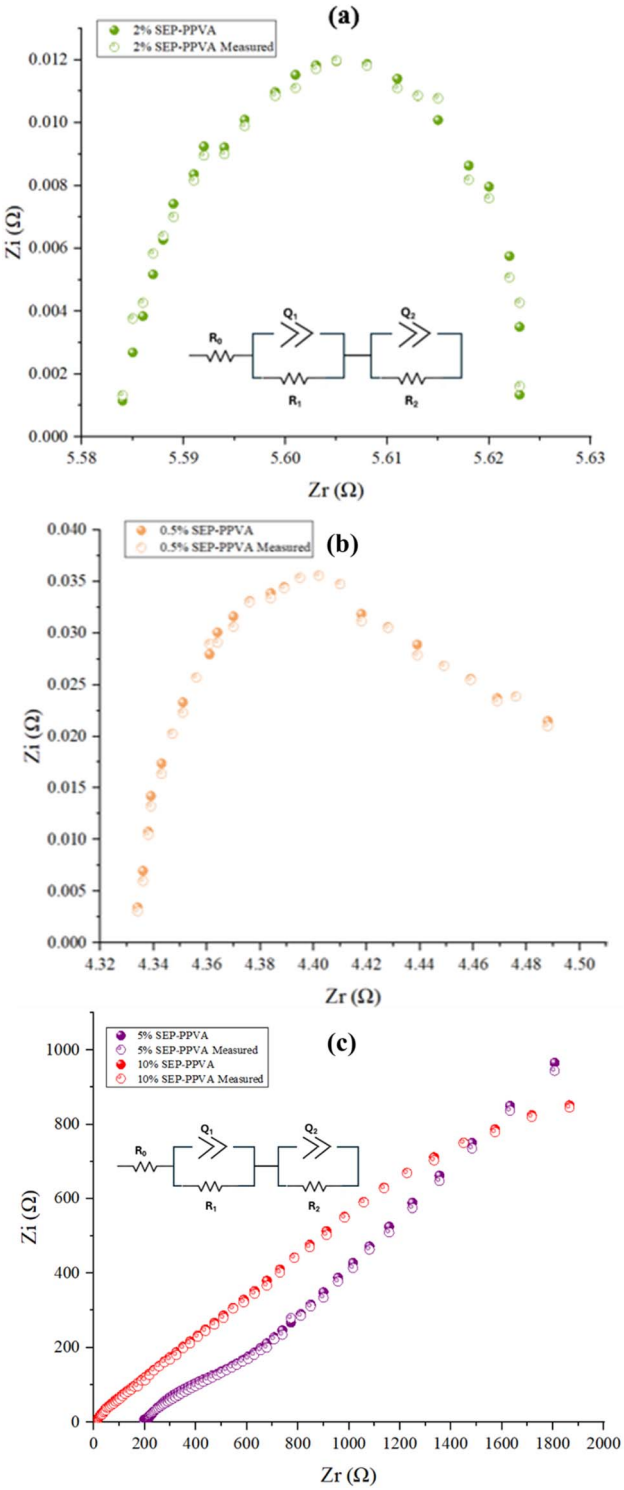

Fig. 13 Equivalent circuit modeling of SEP-PPVA composite membranes (a) 0.5% SEP-PPVA (b) 2% SEP-PPVA (c) 5% SEP-PPVA and 10% SEP-PPVA.

electrode interface through a capacitive double layer. A combination of *R*–*C* elements is represented by a semicircle, whereas a non-ideal capacitance originates a depressed semicircle represented by a constant-phase element (CPE), as follows:

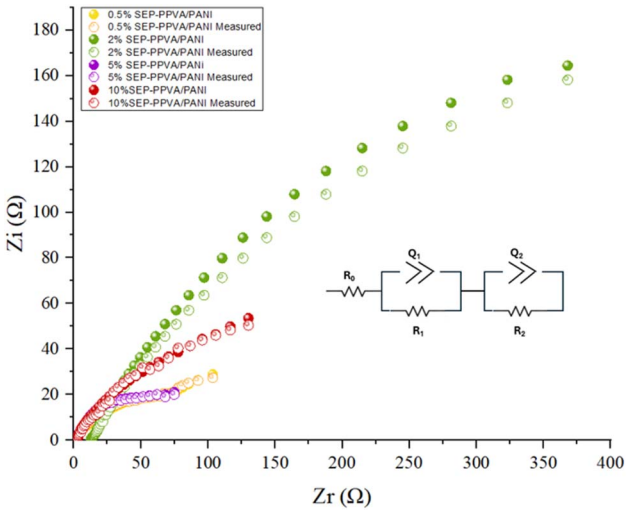

Fig. 14 EIS circuit model and fitting of SEP–PPVA/PANI.

$$Z_c = \frac{1}{Y_0(j\omega)^{\alpha}} \quad (5)$$

where α represents distribution index; $n < 1$ for CPE and $n = 1$ for pure capacitor. The CPE behaviour arises due to electrode or membrane surface irregularities, porosity, reactivity, and current and potential distribution associated with electrolyte and the electrode.[64]

In low frequency domain, another semicircle is shown in all membranes (Fig. 13 and 14) that can be modelled using another *R*–*Q* combination with a larger characteristic time. This may indicate the diffusion of ions through polymer matrix and SEP in the composite membranes (Fig. 12). The charge transfer in the bulk of the membrane is a slower process and highly dependent on SEP concentration in the membrane. This charge transport can be associated with the silanol group (Si–OH) of SEP that has the capability of cation exchange due to its modification and bonding with PPVA.

At 0.5 wt% SEP loading in the PPVA matrix, the resistance (on the Z_r scale) and capacitance (on the Z_i scale) are small, indicating a negligible effect of SEP at this loading. As the SEP content increased (*i.e.*, 5 wt% and 10 wt%), both resistance and capacitance increased (Fig. 13c). The real component of impedance (Z_r) peaks at 5 wt% SEP, compared with 10 wt%, suggested that a threshold SEP loading was required to enhance charge transfer through the filler, likely due to water retention and other concentration-dependent factors. When modeling the charge transfer processes of these SEP–PPVA membranes using an $R_0(RQ)(RQ)$ equivalent circuit, the parameter values also reflected the effects of SEP loading (Table 2). The uncompensated electronic resistance (R_0) showed an inconsistent trend, associated with an inhomogeneous surface and incomplete contact with the electrodes. Y_1 and R_1 in the first *R*–*Q* combination exhibited high-frequency admittance and resistance, respectively, which can be associated with the rapid charge transport mechanism occurring at the membrane/electrode interface. Double-layer capacitive charging at the

Table 2 EIS modelling data of SEP–PPVA and SEP–PPVA/PANI membranes fitted with [$R(QR)(QR)$] type model

	Model parameters							
Membrane identity	R_0	$Q_1(Y_1)$	$Q_1(n_1)$	R_1	$Q_2(Y_2)$	$Q_2(n_2)$	R_2	Chi sq.
0.5% SEP–PPVA	0.05154	0.1972	0.9891	0.07822	1.027	0.996	4.341	8.11×10^{-6}
5% SEP–PPVA	196.8	0.000475	0.7101	580.3	0.000154	0.4384	2509	3.64×10^{-4}
10% SEP–PPVA	7.803	0.000448	0.4696	135.7	8.03×10^{-5}	0.6187	4047	4.18×10^{-3}
0.5% SEP–PPVA/PANI	1.336	6.31×10^{-5}	0.8284	8.787	0.002547	0.4558	105.6	8.51×10^{-3}
2% SEP–PPVA/PANI	12.9	0.002933	0.9623	228.1	0.002381	0.5505	258	6.14×10^{-3}
5% SEP–PPVA/PANI	1.643	0.000922	0.6789	2.94	0.000252	0.8869	75.69	9.17×10^{-3}
10% SEP–PPVA/PANI	2.342	0.000107	0.8269	12.27	0.000497	0.6933	149.2	1.10×10^{-2}

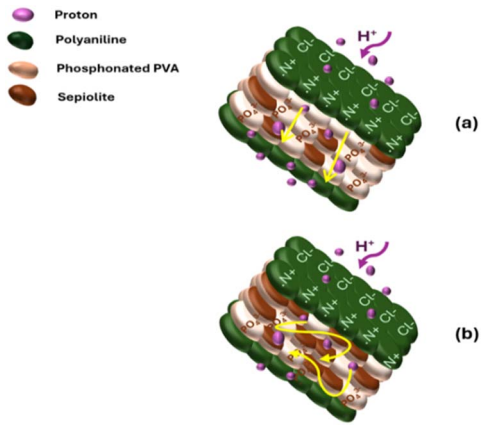

Fig. 15 Proton conduction mechanism, (a) lower SEP concentration (b) higher concentration.

interface showed low admittance (Y_1), with a distributed coefficient (n_1) indicating an inhomogeneous membrane surface as the SEP content increased (Table 2), which is in line with the previous results. The admittance at low frequencies (Y_2) specifies charge transfer within the bulk membrane, where higher R_2 values resulted from ionic conduction through heterogeneous membranes. Y_2 decreased significantly as R_2 increased, indicating a low pseudocapacitance value with increasing SEP content. Strong interfacial interactions, such as hydrogen bonding between $-PO_4^{3-}$ groups and SEP, are responsible for this behavior. The inorganic clay SEP reduces swelling of PPVA membranes, offering increased resistance to proton passage. The proposed mechanism of proton conduction with high and low SEP content in the composite membranes is illustrated in Fig. 15.

Depositing PANI at the surface of SEP–PPVA membranes decreased impedance values, as shown in Fig. 14. The $R_0(R_1Q_1)(R_2Q_2)$ type equivalent circuit fitting results are given in Table 2 indicating a strong influence of PANI deposition on both resistive and capacitive charge transference in the membranes. PANI-coated membranes showed admittance values approximately two orders of magnitude higher than uncoated membranes at low frequencies, showing a dominant charge transfer mechanism facilitated by polaron/bipolaron transitions within PANI. This transition enhanced proton conduction by providing delocalized electronic states that provided smooth charge carrier hopping, alongside the proton-conducting pathways maintained by hydrated SEP and PPVA phosphonate groups.

The EIS results showed that SEP–PANI composite membranes demonstrate synergistic enhancement in charge transfer and proton conduction by the incorporation of SEP and layering of PANI on PPVA membrane. SEP contributed by retaining water and creating proton transport channels *via* silanol groups, whereas PANI improved surface conductivity and electrochemical double-layer behavior through its unique redox-active polymer structure. This synergy resulted in membranes with lower charge transfer resistance, higher capacitive response, and improved suitability for proton exchange membrane fuel cell applications.

Conclusion

This study presents the development of novel SEP–PPVA/PANI composite membranes tailored for proton exchange membrane fuel cell (PEMFC) applications by combining the unique benefits of hygroscopic sepiolite filler and electroactive polyaniline (PANI) surface layering. The incorporation of SEP into PPVA matrix enhanced water retention and mechanical stability through physical crosslinking and strong interfacial hydrogen bonding, which shifted the glass transition temperature (T_g) to a higher temperature and increased storage modulus in dynamic mechanical testing for temperature up to 63 °C. PANI coating further improved proton conductivity by introducing hydrophilic channels and facilitating polaron/bipolaron charge transfer at membrane surface, reducing overall impedance and enhancing electrochemical performance. PPVA–SEP/PANI composite membranes exhibited a maximum proton conductivity of 96 mS cm^{-1} at 5% sepiolite loading under water-soaked conditions, with an ion exchange capacity (IEC) of 2.08 meq. g^{-1} and water uptake 81%, reflecting an optimized balance between hydration and dimensional stability that is critical for efficient PEMFC operation at elevated temperatures. Dynamic mechanical analysis (DMA) showed storage modulus values up to 1600 MPa at 60 °C, indicating thermomechanical stability within typical PEMFC operating ranges, although a decline in the storage (*i.e.*, elastic) modulus beyond this temperature highlighted the need for further optimization for high-temperature durability.

Electrochemical impedance spectroscopy (EIS) analysis confirmed a synergistic effect between sepiolite and PANI, where surface PANI layering decreased membrane resistance and shifted the proton conduction mechanism to the charge transport *via* polaron/bipolaron hopping. This interplay contributes to the composite membranes' improved proton transport pathways and mechanical integrity, positioning them as promising candidates for PEMFC applications requiring stable performance under variable hydration and temperature conditions.

This study shows that the strategic combination of sepiolite as a functional inorganic filler and PANI as an electroactive surface modifier provides a valuable approach for designing high-performance PEMs with tailored water management, mechanical stability, and proton conductivity for next-generation fuel cells. The optimization of PVA phosphonation, SEP content and PANI layering may improve the thermo-mechanical stability and electrochemical performance, coupled with the long-term thermochemical stability (*e.g.*, Fenton's test) may ensure the suitability of these novel membrane systems for PEMFC applications.

Conflicts of interest

The authors declare that they have no conflict of interest.

Data availability

The EIS spectra of individual SEP-PPVA/PANI membranes are available as supplementary information (SI) to this article. Supplementary information is available. See DOI: https://doi.org/10.1039/d5ra09259k.

Acknowledgements

This research was supported by Department of Polymer and Process Engineering, University of Engineering and Technology, Lahore, Pakistan.

References

1 H. Guo, Z. Li, H. Pei, P. Sun, L. Zhang, P. Li and X. Yin, *J. Membr. Sci.*, 2022, **644**, 120092.
2 W. Hwang and Y.-E. Sung, *J. Electrochem. Sci. Technol.*, 2023, **14**, 120–130.
3 X.-M. Li and J. Gao, *SusMat*, 2022, **2**, 504–534.
4 S. Mo, L. Du, Z. Huang, J. Chen, Y. Zhou, P. Wu, L. Meng, N. Wang, L. Xing, M. Zhao, Y. Yang, J. Tang, Y. Zou and S. Ye, *Electrochem. Energy Rev.*, 2023, **6**, 28–67.
5 A. Parekh, *Front. Energy Res.*, 2022, **10**, 956132.
6 L. Trindade, K. Borba, L. Zanchet, D. Lima, A. Trench, F. Rey, U. Diaz, E. Longo, K. Bernardo-Gusmao and E. Martini, *Mater. Chem. Phys.*, 2019, **236**, 121792.
7 Z. Xin, Z. Yanyi and W. Xiaobing, *Energy Rep.*, 2023, **10**, 1943–1950.
8 K. Qiao, H. Liu, S. Huang, X. Zeng and D. Cao, *Int. J. Hydrogen Energy*, 2023, **50**, 209–220.
9 A. L. Chibac-Scutaru and S. Coseri, *Int. J. Biol. Macromol.*, 2023, **247**, 125810.
10 P. Khomein, W. Ketelaars, T. Lap and G. Liu, *Renewable Sustainable Energy Rev.*, 2021, **137**, 110471.
11 J.-H. Wee, *Renewable Sustainable Energy Rev.*, 2007, **11**, 1720–1738.
12 F. C. Teixeira, A. I. de Sá, A. P. S. Teixeira and C. M. Rangel, *Appl. Surf. Sci.*, 2019, **487**, 889–897.
13 S. Roy, A. Ghorai, H. Komber, B. Voit and S. Banerjee, *Eur. Polym. J.*, 2020, **136**, 109898.
14 C. Zhao, B. Li, L. Zhang, Y. Han and X. Wu, *Renewable Energy*, 2023, **215**, 118899.
15 N. Wu, Y. Liu, X. Tian, F. Liu, Y. Ma, S. Zhang, Q. Zhang, D. Hou, Y. Qi, R. Yang and L. Wang, *J. Power Sources*, 2023, **580**, 233412.
16 T. Uenishi and R. Imoto, *J. Power Sources*, 2023, **580**, 233408.
17 S. J. Peighambardoust, S. Rowshanzamir and M. Amjadi, *Int. J. Hydrogen Energy*, 2010, **35**, 9349–9384.
18 T. Jia, S. Shen, J. Zhao, J. Jin, B. Pan, X. Duan, C. Meng and Q. Che, *Int. J. Hydrogen Energy*, 2020, **45**, 14517–14527.
19 W. R. W. Daud, R. E. Rosli, E. H. Majlan, S. A. A. Hamid, R. Mohamed and T. Husaini, *Renewable Energy*, 2017, **113**, 620–638.
20 N. Laconti, H. Liu, C. Mittelsteadt and R. McDonald, *ECS Meet. Abstr.*, 2005, **3**, 647–662.
21 K. Uosaki, K. Okazaki and H. Kita, *J. Electroanal. Chem.*, 1990, **287**, 163–169.
22 K. T. Adjemian, S. Srinivasan, J. Benziger and A. B. Bocarsly, *J. Power Sources*, 2002, **109**, 356–364.
23 Y. M. Kim, S. H. Choi, H. C. Lee, M. Z. Hong, K. Kim and H.-I. Lee, *Electrochim. Acta*, 2004, **49**, 4787–4796.
24 A. Qaiser, M. Hyland and D. Patterson, *J. Phys. Chem. B*, 2009, **113**, 14986–14993.
25 J. Yang, P. K. Shen, J. Varcoe and Z. Wei, *J. Power Sources*, 2009, **189**, 1016–1019.
26 A. F. Elerian, A. A. Mohamed, E. M. Elnaggar, G. Abdel-Naeem and M. A. Abu-Saied, *Polym. Bull.*, 2024, **81**, 17177–17212.
27 T. Tamer, A. Omer, M. Sabet, M. E. Youssef, A. Hashem and M. Mohy Eldin, *Desalin. Water Treat.*, 2021, **227**, 132–148.
28 M. A. Abu-Saied, K. M. Abualnaja, E. A. El-Desouky, G. Abdel-Naeem, E. A. Eldeeb and A. F. Elerian, *Desalin. Water Treat.*, 2024, **320**, 100759.
29 A. Şahin and İ. Ar, *J. Power Sources*, 2015, **288**, 426–433.
30 P. Sun, Z. Li, S. Wang and X. Yin, *J. Membr. Sci.*, 2018, **549**, 660–669.
31 R. Escudero-Cid, M. Montiel, L. Sotomayor, B. Loureiro, E. Fatás and P. Ocón, *Int. J. Hydrogen Energy*, 2015, **40**, 8182–8192.
32 A. Çalı, A. Şahin and İ. Ar, *Can. J. Chem. Eng.*, 2020, **98**, 892–904.
33 W. Mabrouk, K. Charradi, R. Lafi, H. S. AlSalem, H. Maghraoui-Meherzi and S. M. A. S. Keshk, *J. Membr. Sci.*, 2022, **657**, 15331–15339.
34 M. Alkan and R. Benlikaya, *J. Appl. Polym. Sci.*, 2009, **112**, 3764–3774.

35 B. Aziz, G. Abdullah, A. Hussein and M. Ahmed, *Polymers*, 2017, **9**, 622.
36 A. Anis, A. Banthia and S. Bandyopadhyay, *J. Mater. Eng. Perform.*, 2008, **17**, 772–779.
37 X. Sun, S. C. Simonsen, T. Norby and A. Chatzitakis, *Membranes*, 2019, **9**, 83.
38 M. A. Radha, PhD thesis, Selçuk Üniversitesi, 2018.
39 H. Farrokhzad, S. Darvishmanesh, G. Genduso, T. Van Gerven and B. Van der Bruggen, *Electrochim. Acta*, 2015, **158**, 64–72.
40 I. Falina, N. Loza, S. Loza, E. Titskaya and N. Romanyuk, *Membranes*, 2021, **11**, 227.
41 M. S. Malik, A. A. Qaiser and M. A. Arif, *RSC Adv.*, 2016, **6**, 115046–115054.
42 T. Soboleva, Z. Xie, Z. Shi, E. Tsang, T. Navessin and S. Holdcroft, *J. Electroanal. Chem.*, 2008, **622**, 145–152.
43 S.-H. Yun, S.-H. Shin, J.-Y. Lee, S.-J. Seo, S.-H. Oh, Y.-W. Choi and S.-H. Moon, *J. Membr. Sci.*, 2012, **417–418**, 210–216.
44 M. A. Shehzad, A. A. Qaiser, A. Javaid and F. Saeed, *Synth. Met.*, 2015, **200**, 164–171.
45 Z. Wang, H. Zheng, Q. Chen, S. Zhang, F. Yang, J. Kang, J. Chen, Y. Cao and M. Xiang, *J. Polym. Res.*, 2019, **26**, 200.
46 S. Lazarević, I. Janković-Častvan, D. Jovanović, S. Milonjić, D. Janaćković and R. Petrović, *Appl. Clay Sci.*, 2007, **37**, 47–57.
47 M. A. Moreira, K. J. Ciuffi, V. Rives, M. A. Vicente, R. Trujillano, A. Gil, S. A. Korili and E. H. de Faria, *Appl. Clay Sci.*, 2017, **135**, 394–404.
48 A. Xue, S. Zhou, Y. Zhao, X. Lu and P. Han, *J. Hazard. Mater.*, 2011, **194**, 7–14.
49 M. Ahmad, A. A. Qaiser, N. U. Huda and A. Saeed, *RSC Adv.*, 2020, **10**, 3029–3039.
50 H. Pei, L. Hong and J. Y. Lee, *J. Membr. Sci.*, 2008, **307**, 126–135.
51 H. Nagar, N. Sahu, V. V. Basava Rao and S. Sridhar, *Renewable Energy*, 2020, **146**, 1262–1277.
52 H. Lee and S. Kang, *Polymers*, 2020, **12**, 1363.
53 C. Beauger, G. Lainé, A. Burr, A. Taguet, B. Otazaghine and A. Rigacci, *J. Membr. Sci.*, 2013, **430**, 167–179.
54 M. B. K. Niazi, Z. Jahan, S. S. Berg and Ø. W. Gregersen, *Carbohydr. Polym.*, 2017, **177**, 258–268.
55 A. Anis, A. Banthia and S. Bandyopadhyay, *J. Mater. Eng. Perform.*, 2008, **17**, 772–779.
56 C. Y. Wong, W. Y. Wong, K. Ramya, M. Khalid, K. S. Loh, W. R. W. Daud, K. L. Lim, R. Walvekar and A. A. H. Kadhum, *Int. J. Hydrogen Energy*, 2019, **44**, 6116–6135.
57 Y. Zhang, L. Zou, B. P. Ladewig and D. Mulcahy, *Desalination*, 2015, **362**, 59–67.
58 F. G. Üçtuğ and J. Nijem, *Asia-Pac. J. Chem. Eng.*, 2017, **12**, 682–693.
59 H. Beydaghi, M. Javanbakht, A. Bagheri, P. Salarizadeh, H. G. Zahmatkesh, S. Kashefi and E. Kowsari, *RSC Adv.*, 2015, **5**, 74054–74064.
60 R. K. Nagarale, G. S. Gohil and V. K. Shahi, *J. Membr. Sci.*, 2006, **280**, 389–396.
61 C.-C. Yang, *Int. J. Hydrogen Energy*, 2011, **36**, 4419–4431.
62 S. Mollá Romano and V. Compañ Moreno, *J. Power Sources*, 2011, **196**, 2699–2708.
63 J. Alvaro, G. Alfonso, P. Carlos, A. Maria, M. Reyes, M. Cortés, P. Alvaro, M. De, J. Correa and K. Ballestero, *Int. J. Hydrogen Energy*, 2017, **42**, 1561–1570.
64 A. A. Qaiser, M. M. Hyland and D. A. Patterson, *J. Phys. Chem. B*, 2011, **115**, 1652–1661.